

# FGBERT: Function-Driven Pre-trained Gene Language Model for Metagenomics

Chenrui Duan<sup>1,2</sup>, Zelin Zang<sup>1,2</sup>, Yongjie Xu<sup>1,2</sup>, Hang He<sup>2</sup>, Zihan Liu<sup>1,2</sup>, Zijia Song<sup>3</sup>, Jusheng Zheng<sup>2</sup> and Stan Z. Li<sup>\*2</sup>

<sup>1</sup>Zhejiang University

<sup>2</sup>AI Lab, Research Center for Industries of the Future, Westlake University  
{duanchenrui, zangzelin, xuyongjie, hehang, zhengjusheng}@westlake.edu.cn

<sup>3</sup>National University of Defense Technology  
songzijia@nudt.edu.cn

## Abstract

Metagenomic data, comprising mixed multi-species genomes, are prevalent in diverse environments like oceans and soils, significantly impacting human health and ecological functions. However, current research relies on K-mer representations, limiting the capture of structurally relevant gene contexts. To address these limitations and further our understanding of complex relationships between metagenomic sequences and their functions, we introduce a protein-based gene representation as a context-aware and structure-relevant tokenizer. Our approach includes Masked Gene Modeling (MGM) for gene group-level pre-training, providing insights into inter-gene contextual information, and Triple Enhanced Metagenomic Contrastive Learning (TEM-CL) for gene-level pre-training to model gene sequence-function relationships. MGM and TEM-CL constitute our novel metagenomic language model FGBERT, pre-trained on 100 million metagenomic sequences. We demonstrate the superiority of our proposed FGBERT on eight datasets.

## 1 Introduction

Metagenomics, the study of mixed genomes of microbial communities in the environment (e.g. gut microbiomes or soil ecosystems) [37, 39], has revealed the critical role in fundamental biological processes like enzyme synthesis,

gene expression regulation, and immune function [48, 36]. In light of this, deciphering the complex sequences of multiple species in metagenomics is vital for unraveling life’s mechanisms and advancing biotechnology [4, 33, 34].

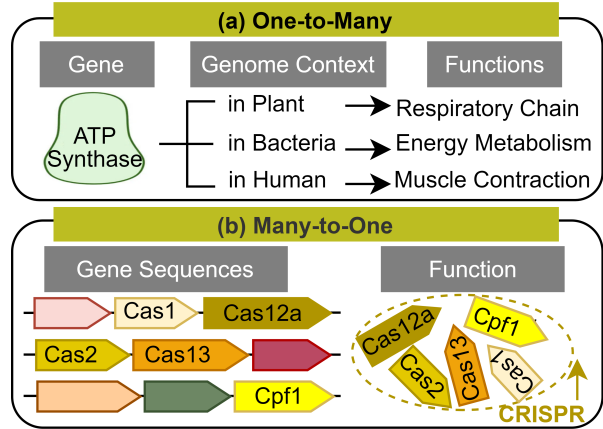


Figure 1: Two types of complex relationships between gene sequences and functions in metagenomics. One-to-Many means that the same gene may display different functions based on the genomic context; for example, ATP synthase works differently in plants, heterotrophic bacteria, and humans. Many-to-One shows that multiple genes may perform the same function; for instance, different genes from different bacteria, e.g., Cpf1, Cas1, etc. produce the same resistance function within the immune system CRISPR.

In metagenomic data analysis, various computational methods have emerged. Traditional alignment-based meth-

\*Corresponding author: Stan.ZQ.Li@westlake.edu.cn

ods rely on homology search against reference genome databases [53]. Machine learning-based methods [20, 31, 42] generally take K-mer as the basic processing unit and adopt its frequency or embedding as the input feature, which proved to be efficient alternatives to traditional methods. Recently, Transformer [57] has been widely used for modeling sequence data due to its ability to capture long-range dependencies. Several pre-trained genomic models [63, 10] utilize Transformer architectures to effectively model complex DNA contexts. However, these models, primarily designed for single-species analysis, face challenges in mixed multi-species metagenomic data. Meta-Transformer [56] and ViBE [18] use K-mer embeddings, cater to specific metagenomic applications, with the former using Transformer for read classification and the latter pre-trained BERT to predict virus classes.

Yet existing genome or metagenomic pre-trained models still face many challenges when dealing with metagenomic data. First, how to encode a gene sequence with biological meaning? Typical pre-processing of genomic data often relies on K-mer to represent a local feature of a gene sequence. However, this approach, with its fixed and limited ‘vocabulary’ of K-mer combinations [63], falls short in capturing informative and global gene representations. Secondly, how to clarify the complicated relationships between gene sequences and their functions in metagenomic analysis? This challenge can be categorized as One-to-Many and Many-to-One problems, as opposed to single-species genome analyses (e.g., identifying regulatory elements in a particular genome). **One-to-Many** problem indicates that a single gene can exhibit various functions in different genomic contexts, underscoring the significance of inter-gene interactions in function regulation [59]. Figure 1a demonstrates that the ATP synthase exhibits specific functionalities in diverse organisms such as bacteria, plants, and humans. Conversely, **Many-to-One** problem implies that different genes can share the same function, emphasizing expression commonality [3]. As shown in Figure 1b, CRISPR [23] is an immune mechanism where different proteins such as Cpf1, Cas1, and Cas13, etc. serve this function.

To address these challenges, we propose FGBERT, a novel metagenomic pre-trained model equipped with the ability to encode contextually-aware and functionally relevant representations of metagenomic sequences. We propose a protein-based gene representation as a context-aware tokenizer to encode each gene sequence, which allows for a flexible token vocabulary for longer metagenomic sequences. This strategy leverages the inherent protein functional and structural information encoded in metagenomic data [48]; and, due to the redundancy of codon-to-amino acid mappings [12], since we adopt the embedding of protein sequences, the function remains unchanged despite po-

tential mutations. With the new tokenizer, we propose a gene group-level pre-training task, named Masked Gene modeling (MGM), to mask some genes randomly and then pre-train a Roberta-like model to predict them, enhancing the understanding of inter-/intra-gene contextual relationships and how the same gene act in different genome contexts in One-to-Many scenarios. Furthermore, we propose Triplet Enhanced Metagenomic Contrastive Learning (TEM-CL) to identify genes with similar functions together with data augmentation and negative sampling module, boosting the model’s ability to recognize commonalities among gene functions in Many-to-One scenarios. MGM and TEM-CL constitute a joint pre-training model, which advances the co-representation learning of metagenomic gene sequences and functions.

**Contributions.** To the best of our knowledge, this is the first metagenomic pre-trained model encoding context-aware and function-relevant representations of metagenomic sequences. To summarize: (1) We introduce a new idea of protein-based gene representations to learn biologically meaningful tokenization of long sequences. (2) Hinged on this idea, we propose MGM to model inter-gene relationships and TEM-CL to learn complex relationships between gene sequences and functions. (3) We conduct extensive experiments on four levels of downstream tasks. Our proposed FGBERT obtains state-of-the-art performance in comparison to a comprehensive suite of baselines.

## 2 Related Works

**Research on Metagenomics** Traditional alignment-based methods like MetaPhlan5 [53], aim to match similarities between query sequences and known reference genomes and are common for taxonomic profiling. Advancements in deep learning have led to new methods like CNN-MGP [2] and DeepVirFinder [49], which use CNNs for gene and viral classifications with one-hot encoding. K-mer tokenization [14], employed in approaches like MDL4Microbiome [30], is a standard for DNA sequence characterization. Additionally, Virtifier [41] maps a nucleotide sequence using a codon dictionary, combined with LSTM to predict viral genes. DeepMicrobes [31] employs a self-attention mechanism, while DeepTE [58] uses K-mer inputs with CNNs for element classification, and Genomicnlp [42] applies word2vec for gene function analysis. Meta-Transformer [56] uses K-mer embedding for species classification with Transformer. For pre-training models, LookingGlass [20] uses a three-layer LSTM model for functional prediction in short DNA reads. ViBE [18] employs a K-mer token-based BERT model pre-trained with Masked Language Modeling (MLM) for virus identification.

**Pre-Training on Genomics** The BERT model, effective

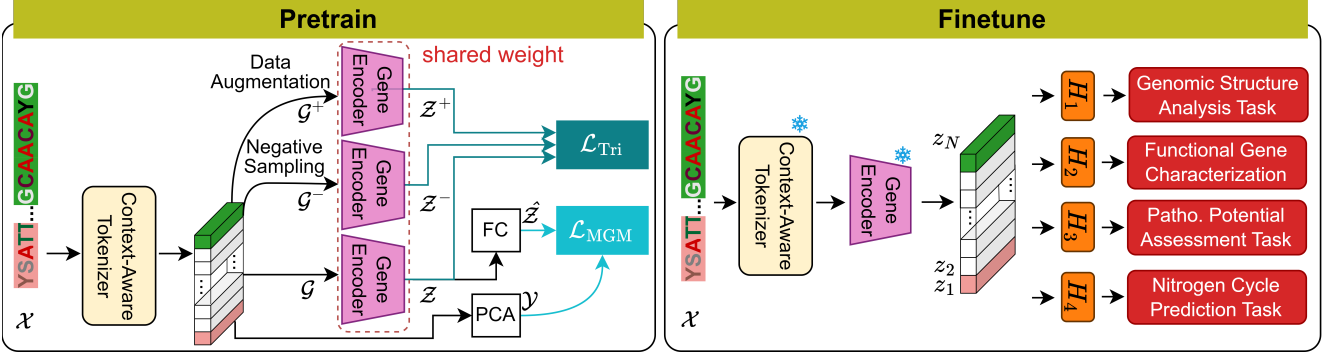


Figure 2: Overview of FGBERT. A metagenomic sequence  $\mathcal{X}$  is converted into ordered protein-based gene representations  $\mathcal{G}$  via a Context-Aware Tokenizer. Next, we pre-train a Gene Encoder with  $\mathcal{L}_{\text{MGM}}$ , 15% of these tokens are masked to predict labels  $\mathcal{Y}$ . Meanwhile, we introduce  $\mathcal{L}_{\text{Tri}}$  to distinguish gene sequences. The data augmentation and negative sampling modules generate positive samples  $\mathcal{G}^+$  and negative samples  $\mathcal{G}^-$ , respectively. Finally, after fine-tuning, FGBERT can handle various downstream tasks.

in DNA sequence characterization, is limited by the Transformer architecture’s computational burden. LOGO [60] addresses this by cutting off long sequences into 1-2kb sub-sequences. Enformer [6] combines extended convolution with Transformers for long human genomic data. GenSLMs [64] introduce hierarchical language models for whole-genome modeling. DNABERT [24], the first pre-trained model on the human genome that focuses on extracting efficient feature representations from gene sequences. DNABERT2 [63], its successor, uses Byte Pair Encoding on multi-species genomic data. NT [10] is trained on nucleotide sequences from human and other species genomes and evaluated on 18 genome prediction tasks. HyenaDNA [43] presents a long-range genome sequence model based on single-nucleotide polymorphisms on the human reference genome.

### 3 Methods

In this section, we detail the proposed pre-training framework FGBERT, which contains MGM and TEM-CL illustrated in Figure 2.

**Notation** Given a metagenomic long sequence  $\mathcal{X}$ , after ultrasonic fragmentation and assembly techniques,  $N$  genes  $\{x_i\}_{i=1}^N$  are obtained, which is tokenized to  $g_i \in \mathbb{R}^d$  together with its corresponding label  $y_i \in \mathbb{R}^{100}$ , where  $d$  is the token dimension. After that, we concatenate  $\{g_i\}_{i=1}^n$  into a gene group  $\mathcal{G}$ . During the pre-training stage, each gene group  $\mathcal{G}$  is passed to the context-aware genome language encoder  $\mathcal{F}(\cdot)$  to obtain knowledge representations  $z_i$  for the input token  $g_i$ , where  $z_i = \mathcal{F}(g_i)$ . Then we apply a fully connected layer to obtain  $\hat{z}_i$  from  $z_i$ , where  $\hat{z}_i = \mathcal{H}(z_i)$ ,  $\mathcal{H}(\cdot)$  is a multi-classification head. Additionally, we integrate contrastive learning. For gene  $x_i$ , we in-

troduce a data augmentation module to construct positive samples  $x_{j(i)}$  and employ hard negative sampling strategy mining for negative sample construction  $x_{k(i)}$ .

#### 3.1 Masked Gene Modeling (MGM)

**Context-aware Tokenizer** To address the first challenge, we propose the protein-based gene representation as a context-aware tokenizer, utilizing the ESM-2 [32] with 15 billion parameters. Naturally, this could be replaced by any Protein Language Model (PLM). This process starts with transforming the DNA sequence  $x_i$  from metagenomic sequences  $\mathcal{X}$  into the protein sequence by ENA software [17]. The AA sequence is then transformed into a 1280D normalized ESM-2 representation. An additional dimension is appended to encode gene orientation, resulting in 1281D gene representation  $g_i$ . These representations are concatenated to form gene groups  $\mathcal{G}$  as shown in Figure 3. The conversion from DNA to AA sequences is motivated by the equivalence of certain degenerate DNA codes (i.e. non-‘ATCG’ symbols in  $\mathcal{X}$ ) when translated into AA, underscoring the rationale for transitioning from DNA to AA sequences for clarity and consistency in representation. The gene-protein relationship inherited in metagenomic data itself [48] could be revealed by ESM-2’s comprehensive training data and protein structural and functional information, and thus ESM-2 representation preserves important intra-gene contextually-aware information. This approach bypasses traditional vocabulary limits and avoids raw sequence processing, this provides the flexibility to analyze longer metagenomic sequences.

**Masked Gene Modeling** With this new tokenizer, we propose MGM to pre-train the Gene Encoder. During pre-training, each token (gene) is masked with a 15% probability and predicted based on its genome context. The loss

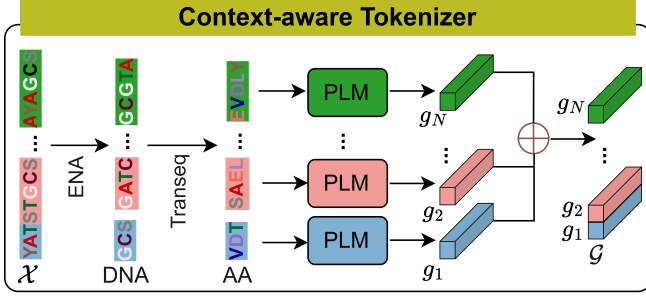


Figure 3: Framework of our proposed Context-Aware Tokenizer.

$\mathcal{L}_{MLM}$  is formulated as a cross-entropy loss:

$$\mathcal{L}_{MLM} = \mathbb{E}_{g \sim \mathcal{G}} \mathbb{E}_M \sum_{i \in M} -\log p(g_i | \mathcal{G}_{/M}) \quad (1)$$

for any given gene representation  $g$ , a random set of indices,  $M$  means the masked gene’s index set, the unmasked gene embeddings  $\mathcal{G}_{/M}$  as the context.

In this way, BERT can learn inter-gene relationships within the genome, contributing to our understanding of gene functionality in diverse genomic contexts in **One-to-Many** scenarios. BERT implicitly learns intra-gene information encapsulated within the PLM representations, further enriching the model’s comprehension of gene characteristics.

What’s more, acknowledging gene polymorphism [47, 62], MGM emphasizes identifying multiple genes that may coexist at a single genomic site, denoted as  $\hat{z}_i = [\hat{z}_1, \hat{z}_2, \hat{z}_3, \hat{z}_4]$ . This necessitates its ability to predict not the individual genes but also various gene combinations within the same site. Hence, two loss functions are combined into  $\mathcal{L}_{MGM}$ :

$$\mathcal{L}_{MGM} = \frac{1}{N} \sum_{i=1}^N \left(1 - \frac{y_i^T \hat{z}_i}{\|y_i\| \cdot \|\hat{z}_i\|}\right)^\gamma + \frac{\alpha}{N} \sum_{i=1}^N \|\hat{z}_i - \tilde{y}_i\|_2^2 \quad (2)$$

where  $\gamma$  is a reconstruction loss with the scaled cosine error, and  $\alpha$  is a weighting factor to balance the importance of the two loss functions. The first item is Feature Reconstruction Loss (FRL), which measures the distance between the model prediction  $\hat{z}_i$  and its corresponding label  $y_i$ . The second item, Probability Prediction Loss (PPL), assesses the discrepancy between the embedding probability  $\tilde{z}_i = \frac{e^{\hat{z}_i}}{\sum_{j=1}^C e^{\hat{z}_j}}$  and the true category probability  $\tilde{y}_i = \frac{e^{y_i}}{\sum_{j=1}^C e^{y_j}}$  processed by the softmax function with  $C$  denoting the number of gene combinations and is set to 4.

### 3.2 Triplet Enhanced Metagenomic Contrastive Learning (TEM-CL)

Although MGM can learn the gene-protein contextual relationship within metagenomic data, we find its ability to

identify sequences with same function to be lacking, which is common in Many-to-One scenarios. During the Enzyme Commission (EC) number annotation of partial metagenomic sequences, we observe that sequences with the same EC number are close to each other in feature space and, vice versa, farther apart. This finding motivates us to adopt a contrastive learning approach to capture the functional relationships between gene classes, enabling different genes with similar functions to cluster together and further optimize model training.

The common contrastive learning objective is to learn an embedding function  $\mathcal{F}$  such that the distance between positive pairs is less than that of negative pairs:  $d(\mathcal{F}(x_a), \mathcal{F}(x_p)) < d(\mathcal{F}(x_a), \mathcal{F}(x_n))$ , where  $d(\cdot, \cdot)$  is a distance function (e.g., Euclidean distance) defined on the embedding space. We adopt SupCon-Hard loss [29] to thus consider multiple positive and negative samples for each anchor, which encourages the model to mine from difficult samples and enhances the robustness and generalization of the model. Additionally, the data augmentation and negative sampling modules are also included to create positive and negative samples and improve the model’s capacity to recognize commonalities among gene classes.

**Triplet Sampling** How to sample the triplets is crucial to learning a well-organized embedding space. For each gene group  $\mathcal{G}$ , as an anchor gene  $x_i$  within a gene batch  $I$ , a mutation strategy is proposed to augment orphan sequences (i.e., functions associated with individual sequences) to generate a large number of pairs of positive samples  $x_{j(i)} \in \mathcal{G}_i^+$  where  $\mathcal{G}_i^+$  is the positive samples set of the anchor  $x_i$ . Concretely, 10 random mutations are performed on each gene sequence, with mutation ratios randomly generated according to a standard normal distribution, and the number of mutations is calculated based on the length of the sequence. This process aims to generate new sequences that are functionally similar to the original sequence but sequentially different, thus providing additional training data for the model and improving the predictive power and accuracy of orphan EC numbers.

**Hard Negatives Sampling** Previous studies [19] have shown that another key to successful contrastive learning is the balance between the triviality and the hardness of the sampled triplets. For the negative sample pair  $x_{k(i)} \in \mathcal{G}_i^-$  where  $\mathcal{G}_i^-$  is the negative samples set of the anchor  $x_i$ .

To begin, we calculate cluster centers for each EC number sequence by averaging the embedded representations of all sequences within the same functional group. These cluster centers represent the centroids of each functional group. Subsequently, we compute Euclidean distances  $d(\cdot)$  based on these centers. When selecting negative samples, we choose samples that are similar to the anchor in latent space but belong to different clusters, rather than randomly selecting them, to increase the challenge of learning. The triplet

loss  $\mathcal{L}_{\text{Tri}}(x_i, \{x_{j(i)}\}_{j=1}^{N_j}, \{x_{k(i)}\}_{k=1}^{N_k})$  is defined as follows:

$$\mathcal{L}_{\text{Tri}} = - \sum_{i \in I} \log \left( \frac{1}{|\mathcal{G}_i^+|} \sum_{j \in \mathcal{G}_i^+} \frac{\exp(S_{z_i, z_{j(i)}}/\tau)}{\mathcal{G}_i} \right) \quad (3)$$

For all negative samples in  $\mathcal{G}_i^-$ , we calculate the weight  $w_{x_k} = \frac{1}{d(x_i, x_k)}$  for each  $x_k \in \mathcal{G}_i^-$  based on its distance relative to anchor  $x_i$ . We then normalize these weights to obtain the probability  $p_{x_k}$ :  $p_{x_k} = \frac{w_{x_k}}{\sum_{x_m \in \mathcal{G}_i^-} w_{x_m}}$ .

$$\mathcal{G}_i = \sum_{x_{j(i)}} \exp(S_{z_i, z_{j(i)}}/\tau) + \sum_{x_{k(i)}} p_{x_k} \exp(S_{z_i, z_{k(i)}}/\tau) \quad (4)$$

where  $\tau$  is the temperature hyper-parameter and  $S$  is the similarity function, typically defined by cosine similarity.

Finally, MGM and TEM-CL constitute a unified pre-training framework with a total loss:

$$\mathcal{L}_{\text{Total}} = \mathcal{L}_{\text{MGM}} + \lambda \mathcal{L}_{\text{Tri}} \quad (5)$$

where  $\lambda$  is a hyper-parameter tuning the influence between two loss functions.

## 4 Experiments

We pre-train FGBERT on a large amount of metagenomic data and comprehensively assess its generalization on different datasets, from thousands to hundreds of thousands, which are described in detail in Table 1. Our goal is to validate the performance of our proposed model on four levels of tasks: (1) Genomic Structure Analysis; (2) Functional Gene Prediction (3) Pathogenicity Potential Assessment and (4) Nitrogen Cycle Prediction.

### 4.1 Pre-training Datasets

We use MGnify updated 2023.02, containing 2,973,257,435 protein sequences. MGnify [50] is a microbial genome dataset that contains genome sequences from different microbial communities. Detailed dataset information is shown in Appendix 5.

### 4.2 Genomic Structure Analysis

**Gene Operons Prediction** is to identify the transcription factor binding sites that have the strongest correlation with operon regulation in the gene regulatory network, which helps us to understand the mechanism and network of gene regulation.

**Dataset.** The transcription factor binding sites with the strongest correlation to the operon in E.coil K12 RegulonDB dataset (E-K12) [51] consists of 4315 operons. Detailed dataset information is listed in Appendix 6.

Table 1: Description of Experimental Datasets. #Seq. and #Class means the number of sequences and categories in each dataset.

| Dataset | Description            | #Seq.   | #Class |
|---------|------------------------|---------|--------|
| E-K12   | Gene Operons           | 4,315   | 1,379  |
| CARD-A  | AMR Gene Family        | 1,966   | 269    |
| CARD-D  | Drug Class             | 1,966   | 37     |
| CARD-R  | Resistance Mechanism   | 1,966   | 7      |
| VFDB    | Virulence Factors      | 8,945   | 15     |
| ENZYME  | Enzyme Functions       | 5,761   | 7      |
| PATRIC  | Pathogenic Genes       | 5,000   | 110    |
| NCycDB  | Nitrogen Cycling Genes | 213,501 | 68     |



Figure 4: Visualization of the attention heatmap from the first head of the last (19th) attention layer. Darker blue color indicates higher attention weight.

**Results.** Table 2 shows that our model achieves the SOTA results for the operon prediction task. From the attention heatmap in Figure 4, it can be observed that gene operon **tolC** has high attention weight with the operons **ygiB** and **ygiC** and **yqiA**. This suggests a significant interaction among these operons, indicating the presence of a shared genetic operon **tolC-ygiB**. Biological research supports that these operons are indeed related to the DUF1190 domain-containing protein YgiB [28].

### 4.3 Functional Gene Prediction

**Antimicrobial Resistance Genes (ARG) Prediction** is crucial for understanding antimicrobial resistance genes and facilitates the identification of resistance mechanisms. However, existing methods suffer from high false-positive rates and specific category bias [26, 5]. Therefore, there is an urgent need for deep learning methods to rapidly and accurately predict the presence of ARG in metagenomic data.

**Dataset.** CARD [25] is a comprehensive ARG database in which each gene is associated with a specific AMR Gene Family (CARD-A: 269 categories in total), Drug Class (CARD-D: 37 categories in total), and Resistance Mechanism (CARD-R: 7 categories in total). Therefore, our model performs a three-category classification prediction task for each gene sequence in CARD, respectively.

Table 2: Macro F1 score(%  $\uparrow$ ) and Weighted F1 score(%  $\uparrow$ ) of our model on eight downstream tasks compared to baselines, including Gene Operon Prediction on E-K12, Antimicrobial Resistance Gene Prediction on three CARD categories (AMR gene family, Drug class, and Resistance mechanism), Virulence Factors Classification on VFDB, Enzyme Function Annotation on ENZYME, Microbial Pathogens Detection on PATRIC, and Nitrogen Cycle Processes Prediction on NCycDB. RF denotes Random Forest, and VT represents Vanilla Transformer.

| Method      | Operons     |             | ARG Prediction |             |             |             |             |             | Virus       |             | Enzyme      |             | Pathogen    |             | N-Cycle     |             |
|-------------|-------------|-------------|----------------|-------------|-------------|-------------|-------------|-------------|-------------|-------------|-------------|-------------|-------------|-------------|-------------|-------------|
|             | E-K12       |             | CARD-A         |             | CARD-D      |             | CARD-R      |             | VFDB        |             | ENZYME      |             | PATRIC      |             | NCycDB      |             |
|             | M.F1        | W.F1        | M.F1           | W.F1        | M.F1        | W.F1        | M.F1        | W.F1        | M.F1        | W.F1        | M.F1        | W.F1        | M.F1        | W.F1        | M.F1        | W.F1        |
| RF          | 20.2        | 34.8        | 22.4           | 35.3        | 36.1        | 49.0        | 47.8        | 57.6        | 22.4        | 38.5        | 33.6        | 41.2        | 25.3        | 29.8        | 67.0        | 71.7        |
| SVM         | 38.6        | 45.2        | 27.6           | 40.5        | 33.6        | 47.2        | 43.3        | 66.2        | 28.0        | 41.4        | 31.3        | 43.6        | 26.6        | 31.2        | 66.9        | 70.3        |
| KNN         | 39.9        | 41.0        | 36.9           | 54.4        | 36.4        | 51.3        | 36.2        | 63.5        | 27.3        | 47.1        | 31.4        | 42.9        | 11.0        | 27.4        | 68.8        | 73.2        |
| LSTM        | 40.4        | 42.5        | 47.1           | 60.3        | 39.1        | 62.3        | 47.5        | 84.2        | 36.7        | 66.3        | 42.8        | 51.0        | 41.3        | 49.7        | 71.9        | 81.2        |
| BiLSTM      | 38.2        | 43.8        | 47.4           | 61.9        | 43.5        | 58.1        | 58.9        | 80.3        | 46.1        | 72.1        | 38.7        | 50.2        | 43.3        | 48.5        | 82.0        | 88.4        |
| VT          | 43.3        | 47.8        | 57.1           | 70.0        | 49.8        | 68.1        | 55.7        | 86.4        | 58.0        | 81.0        | 68.2        | 75.8        | 49.8        | 57.3        | 84.5        | 90.7        |
| HyenaDNA    | 42.4        | 47.1        | 50.9           | 68.2        | 53.6        | 78.1        | 66.2        | 88.1        | 61.0        | 70.4        | 79.6        | 83.6        | 51.1        | 57.6        | 92.4        | 96.0        |
| ESM-2       | 38.2        | 42.5        | 57.2           | 71.4        | 56.0        | 82.1        | 68.2        | 90.0        | 60.7        | 84.4        | 92.5        | 96.7        | 56.0        | 67.5        | 95.8        | 96.1        |
| NT          | 45.1        | 44.8        | 58.5           | 72.0        | 56.2        | 80.2        | 68.0        | 90.3        | 58.3        | 71.6        | 74.1        | 76.7        | 46.1        | 61.9        | 75.1        | 86.5        |
| DNABERT2    | 51.7        | 52.4        | 65.2           | 79.8        | 51.5        | 78.7        | 61.2        | 88.6        | 58.2        | 82.3        | 85.4        | 85.2        | 52.9        | 60.6        | 88.6        | 95.7        |
| <b>Ours</b> | <b>61.8</b> | <b>65.4</b> | <b>78.6</b>    | <b>90.1</b> | <b>57.4</b> | <b>85.2</b> | <b>69.4</b> | <b>91.4</b> | <b>75.7</b> | <b>90.2</b> | <b>99.1</b> | <b>98.8</b> | <b>99.3</b> | <b>99.0</b> | <b>99.5</b> | <b>99.2</b> |

**Results.** The prediction on CARD-A category is especially noteworthy in Table 2. Because this category covers up to 269 different classifications, resulting in a long-tail issue. This requires the model to understand the biological properties of gene sequences and accurately annotate the sequences [40]. To address the long-tail problem, we adjust the data sampling strategy to increase the sampling frequency of fewer samples to improve the model’s prediction accuracy. Table 3 demonstrates the prediction accuracy of FGBERT on CARD-R category. This result shows that our model has better classification results for both majority and minority classes with more than 85% accuracy. Appendix 11 shows that FGBERT has better classification performance for all 269 categories of AMR Gene Family, with 100% data classification accuracy for majority categories such as CTX, ADC, CMY, etc. and minority categories such as AXC, CRH, KLUC, and so on.

Table 3: Detailed Classification Results of FGBERT Model on Resistance Mechanism Category Prediction, including the total number of categories, the number of correct predictions, and the accuracy rate for each class.

| Class Name                    | Total Count | Correct Num | Correct Ratio |
|-------------------------------|-------------|-------------|---------------|
| Antibiotic Inactivation       | 252         | 238         | 94.44%        |
| Antibiotic Target Alteration  | 70          | 59          | 84.29%        |
| Antibiotic Target Protection  | 28          | 27          | 96.43%        |
| Antibiotic Efflux             | 25          | 18          | 72.00%        |
| Antibiotic Target Replacement | 14          | 12          | 85.72%        |

**Virulence Factors (VF) Prediction** is to detect microbial elements like bacterial toxins, which enhance pathogen infectivity and exacerbate antimicrobial resistance. Exist-

ing methods for analyzing metagenomic analyses are insufficient, especially tools for co-predicting ARGs and VFs are scarce, and also suffer from threshold sensitivity [61].

**Dataset.** VFDB [8] dataset includes the major VFs of the most characterized bacterial pathogens, as well as the structural features, functions, and mechanisms of these pathogens. We use VFDB core dataset, including 8945 VF sequences and 15 VF categories.

**Results.** According to the results reported in Table 2, our model achieves the SOTA results on VFDB. Compared to the genomic pre-trained model, our advantage is relatively obvious. For example, M.F1 improves by 30% and W.F1 improves by 9.5% compared to DNABERT2. This further highlights the challenge of directly transferring the genome pre-trained model to the metagenomic domain for precise functional annotation. Conversely, ESM-2, as a PLM, outperformed the genome pre-trained model, emphasizing the significance of harnessing the inherent protein information within metagenomic data.

**Enzyme Function Prediction** is critical for understanding metabolism and disease mechanisms in organisms. While traditional methods rely on time-consuming and labor-intensive biochemical experiments, advanced technologies can be used to efficiently and accurately predict large-scale genomic data.

**Dataset.** ENZYME [7] is a repository of information related to the nomenclature of enzymes. We organize 5761 data, 7 categories of ENZYME core dataset, each enzyme has a unique EC number [44].

**Results.** Our experimental results demonstrate FGBERT’s superior performance on ENZYME dataset. It outperforms ESM-2, the second-highest method, by approximately 6.62% in M.F1 and 2.09% in W.F1, demonstrating

its ability to discern distinct enzyme function characteristics. This observation highlights that our model not only captures gene-protein contextual relationships but also effectively models the relationships between sequences and functions within metagenomic data.

#### 4.4 Pathogenicity Potential Assessment

**Genome Pathogens Prediction** is to assess the pathogenic potential of pathogens to cope with the public health risks caused by newly emerging pathogens. Hence, the development of accurate deep-learning algorithms for the precise identification of pathogens can improve the ability to respond to the threat of drug resistance.

**Dataset.** We use PATRIC core dataset [15], which has 5000 pathogenic bacterial sequences and 110 pathogenic bacterial classes.

**Results.** Table 2 displays the classification results for pathogenic bacteria species on PATRIC. The result shows that FGBERT can recognize key features of genera, resulting in better classification results than baselines. PATRIC dataset, which consists of a large number of categories with relatively fewer data, poses a challenge for models. Due to this complexity, baselines underperform, as they typically require more data to discern the subtle differences between numerous categories. In contrast, FGBERT stands out with M.F1 and W.F1 scores of 99.27% and 99.03% respectively, and appears to be robust against such data scarcity and category abundance, indicating an advanced learning capability suited for high-dimensional classification tasks. This observation highlights the advantage of leveraging protein-based gene representations for improved accuracy in functional annotation tasks.

#### 4.5 Nitrogen Cycle Prediction

**Nitrogen Cycling Process Prediction** is to quantitatively study the functional genes related to the N cycle and linking them to environmental and ecological processes is one of the important focuses in environmental genomics research.

**Dataset.** NCycDB [55] contains a total of 68 genes (sub)families and covers eight N cycle processes with 213501 representative sequences at 100% identity cutoffs, each of which involves a specific gene family and is critical for environmental and ecosystem nitrogen homeostasis.

**Results.** Table 2 presents the classification results of FGBERT on NCycDB. The findings suggest that FGBERT can recognize important features of a particular N cycle and improve gene family classification by recognizing domains. On NCycDB, which consists of a substantial 210,000 data from 68 categories, we observe that the baselines perform comparatively better than on PATRIC. This is due to the

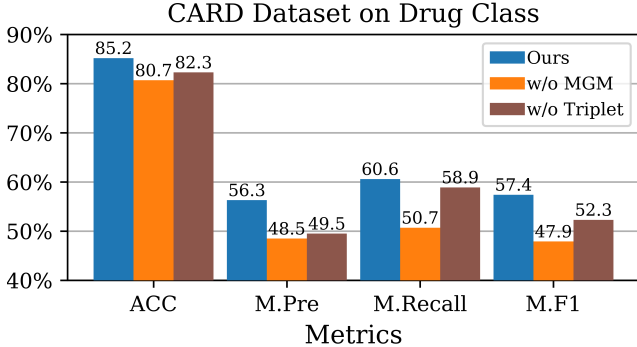


Figure 5: Ablation studies of proposed modules on four downstream tasks.

Table 4: Ablation study to investigate the effectiveness of our proposed modules. “(w/o.) MGM” denotes FGBERT without the MGM and “(w/o.) Triplet” denotes FGBERT without the TEM-CL module, respectively.

| Method        | Operons     | ARG Prediction |             |             |
|---------------|-------------|----------------|-------------|-------------|
|               | E-K12       | CARD-A         | CARD-D      | CARD-R      |
| <b>FGBERT</b> | <b>61.8</b> | <b>78.7</b>    | <b>57.4</b> | <b>69.4</b> |
| w/o. MGM      | -8.1        | -6.7           | -10.5       | -6.7        |
| w/o. Triplet  | -7.4        | -5.4           | -5.8        | -3.4        |

larger data size per category, which allows baselines to better discriminate between the diverse categories, while FGBERT still outperforms with remarkable M.F1 and W.F1 scores of 99.49% and 99.22%, respectively. However, the pre-trained baselines take more time and larger memory for the tokenization process for large datasets, which is analyzed in Sec 4.7.

#### 4.6 Ablation Study

We perform the ablation study to investigate the effectiveness of our proposed components. Table 4 shows the performance of “FGBERT (w/o.) MGM” and “FGBERT (w/o.) Triplet”, respectively on four datasets. Additionally, Figure 5 illustrates four more metrics on CARD dataset. We notice a decrease in M.F1 after removing the MGM and TEM-CL respectively, highlighting their roles in enhancing model performance across different tasks. While TEM-CL contributes to performance, it is evident that MGM has a more substantial impact.

Furthermore, we perform a visualization experiment to validate the effectiveness of MGM in One-to-Many scenario. ATP synthases can exhibit different functions in different organisms to adapt to their respective environmental conditions, even though the basic functions are the same [22]. To explore this, we collect 1177 ATP synthase sequences from UniProt [1] and color them accord-

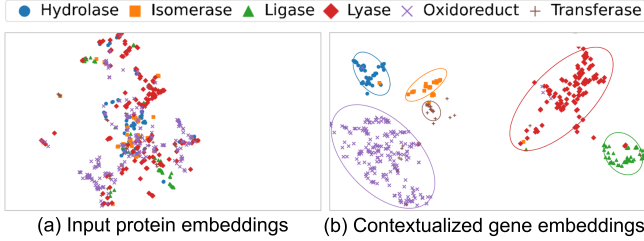


Figure 6: t-SNE visualization of input protein embeddings and our proposed protein-based gene embeddings for ATP synthase sequences ( $n=1177$ ). Each icon denotes an ATP synthase sequence and is colored according to different functions.

ing to six taxonomies, i.e. Hydrolases (35.6%, dark green), Isomerases (3.6%, orange), Ligases (35.7%, blue), Lyases (10.7%, pink), Oxidoreduct (8.9%, light green) and Transferases (5.3%, yellow) (numbers in parentheses indicate category ratios). Figure 6a shows the clustering results of ATPase protein embeddings without genome contextual analysis, indicating that more dispersed clustering results of genes in different genome contexts. Figure 6b presents the clustering results of ATPase embedding after our designed protein-based gene embedding, which shows genes belonging to the same category (in the same color) apparently cluster together. Concretely, Isomerases (3.5%, orange) and Transferases (5.3%, yellow), which account for the smallest percentage, cluster together, whereas, in the left plot, these two are scattered. This demonstrates that our proposed MGM can resolve the One-to-Many relationship between sequences and functions.

#### 4.7 Model Efficiency Study

We analyze the time complexity and memory efficiency of token processing for ours and four genome pre-trained

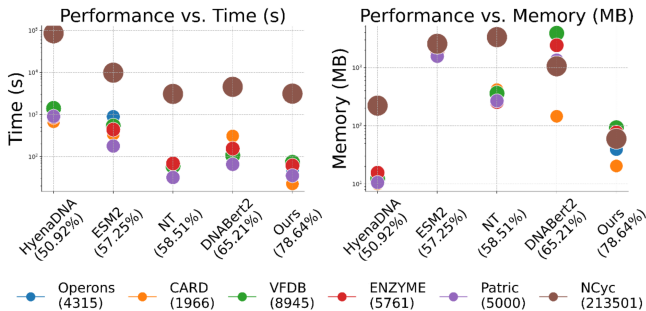


Figure 7: Comparative Analysis on Tokenization Efficiency: Balancing Time(s) vs. Memory Usage(MB). Each circle point on the plot corresponds to a specific dataset, with the point size indicating the dataset’s scale.

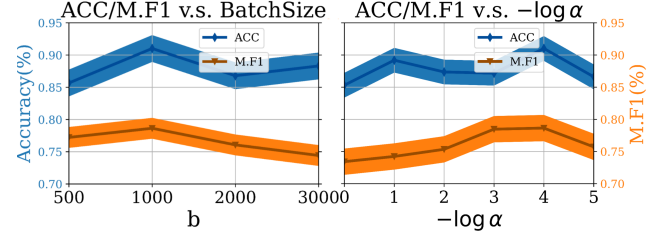


Figure 8: Sensitivity w.r.t Hyper-parameters  $\alpha, b$  of CARD dataset on AMR Gene Family.

methods on six datasets in Figure 7. Our tokenizer achieves the best balance between time, computation, and performance (M.F1) on all datasets. Notably, for NCyc dataset (brown circle) with 213,501 sequences, ours exhibits a remarkable reduction in time by 31.05% compared to DNABERT2 along with a substantial decrease in memory usage by 94.33%. Additionally, for CARD dataset (orange circle) containing 1,966 sequences, ours showcases a significant reduction in time by 61.70% compared to DNABERT2 accompanied by a substantial decrease in memory usage by 58.53%. Although HyenaDNA has a smaller memory footprint than ours on the Operons, CARD, VFDB, and ENZYME datasets, it performs worse than ours in terms of time cost, and performance.

#### 4.8 Sensitivity Analysis

Our sensitivity analysis on the batch size  $b$  indicates that the proposed model can be optimized effectively using small batches without larger performance degradation shown in Figure 8. This observation is particularly important for resource-constrained scenarios, highlighting our model maintains good performance even with limited data. We select a moderate batch size 1000 that balances computational efficiency and model performance. Next, we analyze another hyper-parameter of balance ratio  $\alpha$  on CARD dataset. FGBERT obtains good performance for different values of  $\alpha$ , demonstrating its robustness and insensitivity to this hyper-parameter. We select  $\alpha$  to be 0.4.

### 5 Conclusion

In this paper, we propose a new idea of protein-based gene representation, preserving essential biological characteristics within each gene sequence. With the new context-aware tokenizer, we propose MGM, a gene group-level pre-training task, designed to learn the interactions between genes. Additionally, we develop TEM-CL, a contrastive learning module to generate multiple positive and negative samples to distinguish the gene sequences. MGM and TEM-CL constitute a joint pre-training model, FGBERT for metagenomic data. Our experiments and visualizations



demonstrate the superior performance of our model. For the future, it remains to be explored how to incorporate multi-omics data, such as metabolomics, into our metagenomic pre-trained model.

## References

- [1] Uniprot: the universal protein knowledgebase in 2023. *Nucleic Acids Research*, 51(D1):D523–D531, 2023.
- [2] A. Al-Ajlan and A. El Allali. Cnn-mgp: convolutional neural networks for metagenomics gene prediction. *Interdisciplinary Sciences: Computational Life Sciences*, 11:628–635, 2019.
- [3] B. Al-Shayeb, P. Skopintsev, K. M. Soczek, E. C. Stahl, Z. Li, E. Groover, D. Smock, A. R. Eggers, P. Pausch, B. F. Cress, et al. Diverse virus-encoded crisper-cas systems include streamlined genome editors. *Cell*, 185(24):4574–4586, 2022.
- [4] M. Albertsen. Long-read metagenomics paves the way toward a complete microbial tree of life. *Nature Methods*, 20(1):30–31, 2023.
- [5] B. J. Arnold, I.-T. Huang, and W. P. Hanage. Horizontal gene transfer and adaptive evolution in bacteria. *Nature Reviews Microbiology*, 20(4):206–218, 2022.
- [6] Ž. Avsec, V. Agarwal, D. Visentin, J. R. Ledsam, A. Grabska-Barwinska, K. R. Taylor, Y. Assael, J. Jumper, P. Kohli, and D. R. Kelley. Effective gene expression prediction from sequence by integrating long-range interactions. *Nature methods*, 18(10):1196–1203, 2021.
- [7] A. Bairoch. The enzyme database in 2000. *Nucleic acids research*, 28(1):304–305, 2000.
- [8] L. Chen, J. Yang, J. Yu, Z. Yao, L. Sun, Y. Shen, and Q. Jin. Vfdb: a reference database for bacterial virulence factors. *Nucleic acids research*, 33(suppl\_1):D325–D328, 2005.
- [9] Q. Cui, Z. Yu, Y. Pan, E. O. Purisima, and E. Wang. Micrnas preferentially target the genes with high transcriptional regulation complexity. *Biochemical and biophysical research communications*, 352(3):733–738, 2007.
- [10] H. Dalla-Torre, L. Gonzalez, J. Mendoza-Revilla, N. L. Carranza, A. H. Grzywaczewski, F. Oteri, C. Dallago, E. Trop, B. P. de Almeida, H. Sirelkhatim, et al. The nucleotide transformer: Building and evaluating robust foundation models for human genomics. *bioRxiv*, pages 2023–01, 2023.
- [11] J. Devlin, M.-W. Chang, K. Lee, and K. Toutanova. Bert: Pre-training of deep bidirectional transformers for language understanding. *arXiv preprint arXiv:1810.04805*, 2018.
- [12] D. J. D’Onofrio and D. L. Abel. Redundancy of the genetic code enables translational pausing. *Frontiers in genetics*, 5:140, 2014.
- [13] M. D. Ermolaeva, O. White, and S. L. Salzberg. Prediction of operons in microbial genomes. *Nucleic acids research*, 29(5):1216–1221, 2001.
- [14] A. Fiannaca, L. La Paglia, M. La Rosa, G. Lo Bosco, G. Renda, R. Rizzo, S. Gaglio, and A. Urso. Deep learning models for bacteria taxonomic classification of metagenomic data. *BMC bioinformatics*, 19:61–76, 2018.
- [15] J. J. Gillespie, A. R. Wattam, S. A. Cammer, J. L. Gabbard, M. P. Shukla, O. Dalay, T. Driscoll, D. Hix, S. P. Mane, C. Mao, et al. Patric: the comprehensive bacterial bioinformatics resource with a focus on human pathogenic species. *Infection and immunity*, 79(11):4286–4298, 2011.
- [16] N. Gruber and J. N. Galloway. An earth-system perspective of the global nitrogen cycle. *Nature*, 451(7176):293–296, 2008.
- [17] M. Gruenstaedl. annnex2embl: automatic preparation of annotated dna sequences for bulk submissions to ena. *Bioinformatics*, 36(12):3841–3848, 2020.
- [18] H.-J. Gwak and M. Rho. Vibe: a hierarchical bert model to identify eukaryotic viruses using metagenome sequencing data. *Briefings in Bioinformatics*, 23(4):bbac204, 2022.
- [19] A. Hermans, L. Beyer, and B. Leibe. In defense of the triplet loss for person re-identification. *arXiv preprint arXiv:1703.07737*, 2017.
- [20] A. Hoarfrost, A. Aptekmann, G. Farfañuk, and Y. Bromberg. Deep learning of a bacterial and archaeal universal language of life enables transfer learning and illuminates microbial dark matter. *Nature communications*, 13(1):2606, 2022.
- [21] S. Hochreiter and J. Schmidhuber. Long short-term memory. *Neural computation*, 9(8):1735–1780, 1997.
- [22] S. Hong and P. L. Pedersen. Atp synthase and the actions of inhibitors utilized to study its roles in human health, disease, and other scientific areas. *Microbiology and molecular biology reviews*, 72(4):590–641, 2008.

- [23] Y. Hu, Y. Chen, J. Xu, X. Wang, S. Luo, B. Mao, Q. Zhou, and W. Li. Metagenomic discovery of novel crispr-cas13 systems. *Cell Discovery*, 8(1):107, 2022.
- [24] Y. Ji, Z. Zhou, H. Liu, and R. V. Davuluri. Dnabert: pre-trained bidirectional encoder representations from transformers model for dna-language in genome. *Bioinformatics*, 37(15):2112–2120, 2021.
- [25] B. Jia, A. R. Raphenya, B. Alcock, N. Waglechner, P. Guo, K. K. Tsang, B. A. Lago, B. M. Dave, S. Pereira, A. N. Sharma, et al. Card 2017: expansion and model-centric curation of the comprehensive antibiotic resistance database. *Nucleic acids research*, page gkw1004, 2016.
- [26] Z. Jian, L. Zeng, T. Xu, S. Sun, S. Yan, L. Yang, Y. Huang, J. Jia, and T. Dou. Antibiotic resistance genes in bacteria: Occurrence, spread, and control. *Journal of basic microbiology*, 61(12):1049–1070, 2021.
- [27] K. E. Jones, N. G. Patel, M. A. Levy, A. Storeygard, D. Balk, J. L. Gittleman, and P. Daszak. Global trends in emerging infectious diseases. *Nature*, 451(7181):990–993, 2008.
- [28] P. D. Karp, R. Billington, R. Caspi, C. A. Fulcher, M. Latendresse, A. Kothari, I. M. Keseler, M. Krummenacker, P. E. Midford, Q. Ong, et al. The biocyc collection of microbial genomes and metabolic pathways. *Briefings in bioinformatics*, 20(4):1085–1093, 2019.
- [29] P. Khosla, P. Teterwak, C. Wang, A. Sarna, Y. Tian, P. Isola, A. Maschinot, C. Liu, and D. Krishnan. Supervised contrastive learning. *Advances in neural information processing systems*, 33:18661–18673, 2020.
- [30] S. J. Lee and M. Rho. Multimodal deep learning applied to classify healthy and disease states of human microbiome. *Scientific Reports*, 12(1):824, 2022.
- [31] Q. Liang, P. W. Bible, Y. Liu, B. Zou, and L. Wei. Deepmicrobes: taxonomic classification for metagenomics with deep learning. *NAR Genomics and Bioinformatics*, 2(1):lqaa009, 2020.
- [32] Z. Lin, H. Akin, R. Rao, B. Hie, Z. Zhu, W. Lu, N. Smetanin, A. dos Santos Costa, M. Fazel-Zarandi, T. Sercu, S. Candido, et al. Language models of protein sequences at the scale of evolution enable accurate structure prediction. *bioRxiv*, 2022.
- [33] Z. Lin, H. Akin, R. Rao, B. Hie, Z. Zhu, W. Lu, N. Smetanin, R. Verkuil, O. Kabeli, Y. Shmueli, et al. Evolutionary-scale prediction of atomic-level protein structure with a language model. *Science*, 379(6637):1123–1130, 2023.
- [34] S. Liu, C. D. Moon, N. Zheng, S. Huws, S. Zhao, and J. Wang. Opportunities and challenges of using metagenomic data to bring uncultured microbes into cultivation. *Microbiome*, 10(1):76, 2022.
- [35] I. Loshchilov and F. Hutter. Decoupled weight decay regularization. *arXiv preprint arXiv:1711.05101*, 2017.
- [36] H. Lu, D. J. Diaz, N. J. Czarnecki, C. Zhu, W. Kim, R. Shroff, D. J. Acosta, B. R. Alexander, H. O. Cole, Y. Zhang, et al. Machine learning-aided engineering of hydrolases for pet depolymerization. *Nature*, 604(7907):662–667, 2022.
- [37] S. S. Mande, M. H. Mohammed, and T. S. Ghosh. Classification of metagenomic sequences: methods and challenges. *Briefings in bioinformatics*, 13(6):669–681, 2012.
- [38] J. L. Martínez and F. Baquero. Interactions among strategies associated with bacterial infection: pathogenicity, epidemicity, and antibiotic resistance. *Clinical microbiology reviews*, 15(4):647–679, 2002.
- [39] A. Mathieu, M. Leclercq, M. Sanabria, O. Perin, and A. Droit. Machine learning and deep learning applications in metagenomic taxonomy and functional annotation. *Frontiers in Microbiology*, 13:811495, 2022.
- [40] A. G. McArthur, N. Waglechner, F. Nizam, A. Yan, M. A. Azad, A. J. Baylay, K. Bhullar, M. J. Canova, G. De Pascale, L. Ejim, et al. The comprehensive antibiotic resistance database. *Antimicrobial agents and chemotherapy*, 57(7):3348–3357, 2013.
- [41] Y. Miao, F. Liu, T. Hou, and Y. Liu. Virtifier: a deep learning-based identifier for viral sequences from metagenomes. *Bioinformatics*, 38(5):1216–1222, 2022.
- [42] D. Miller, A. Stern, and D. Burstein. Deciphering microbial gene function using natural language processing. *Nature Communications*, 13(1):5731, 2022.
- [43] E. Nguyen, M. Poli, M. Faizi, A. Thomas, C. Birch-Sykes, M. Wornow, A. Patel, C. Rabideau, S. Marsaroli, Y. Bengio, et al. Hyenadna: Long-range genomic sequence modeling at single nucleotide resolution. *arXiv preprint arXiv:2306.15794*, 2023.

- [44] E. Nomenclature. Recommendations of the nomenclature committee of the international union of biochemistry and molecular biology on the nomenclature and classification of enzymes, 1992.
- [45] J. O’Neill. Tackling drug-resistant infections globally: final report and recommendations. 2016.
- [46] S. Park, Y. Koh, H. Jeon, H. Kim, Y. Yeo, and J. Kang. Enhancing the interpretability of transcription factor binding site prediction using attention mechanism. *Scientific reports*, 10(1):13413, 2020.
- [47] T. Pastinen, B. Ge, and T. J. Hudson. Influence of human genome polymorphism on gene expression. *Human molecular genetics*, 15(suppl\_1):R9–R16, 2006.
- [48] G. A. Pavlopoulos, F. A. Baltoumas, S. Liu, O. Selvitopi, A. P. Camargo, S. Nayfach, A. Azad, S. Roux, L. Call, N. N. Ivanova, et al. Unraveling the functional dark matter through global metagenomics. *Nature*, 622(7983):594–602, 2023.
- [49] J. Ren, K. Song, C. Deng, N. A. Ahlgren, J. A. Fuhrman, Y. Li, X. Xie, R. Poplin, and F. Sun. Identifying viruses from metagenomic data using deep learning. *Quantitative Biology*, 8:64–77, 2020.
- [50] L. Richardson, B. Allen, G. Baldi, M. Beracochea, M. L. Bileschi, T. Burdett, J. Burgin, J. Caballero-Pérez, G. Cochrane, L. J. Colwell, et al. Mgnify: the microbiome sequence data analysis resource in 2023. *Nucleic Acids Research*, 51(D1):D753–D759, 2023.
- [51] H. Salgado, I. Martínez-Flores, V. H. Bustamante, K. Alquicira-Hernández, J. S. García-Sotelo, D. García-Alonso, and J. Collado-Vides. Using regulondb, the escherichia coli k-12 gene regulatory transcriptional network database. *Current protocols in bioinformatics*, 61(1):1–32, 2018.
- [52] M. Schuster and K. K. Paliwal. Bidirectional recurrent neural networks. *IEEE transactions on Signal Processing*, 45(11):2673–2681, 1997.
- [53] N. Segata, L. Waldron, A. Ballarini, V. Narasimhan, O. Jousson, and C. Huttenhower. Metagenomic microbial community profiling using unique clade-specific marker genes. *Nature methods*, 9(8):811–814, 2012.
- [54] O. K. Tawfik and D. S. Enzyme promiscuity: a mechanistic and evolutionary perspective. *Annual review of biochemistry*, 79:471–505, 2010.
- [55] Q. Tu, L. Lin, L. Cheng, Y. Deng, and Z. He. Ncy-cdb: a curated integrative database for fast and accurate metagenomic profiling of nitrogen cycling genes. *Bioinformatics*, 35(6):1040–1048, 2019.
- [56] A. Wichmann, E. Buschong, A. Müller, D. Jünger, A. Hildebrandt, T. Hankeln, and B. Schmidt. Meta-transformer: deep metagenomic sequencing read classification using self-attention models. *NAR Genomics and Bioinformatics*, 5(3):lqad082, 2023.
- [57] T. Wolf, L. Debut, V. Sanh, J. Chaumond, C. Delangue, A. Moi, P. Cistac, T. Rault, R. Louf, M. Funtowicz, et al. Transformers: State-of-the-art natural language processing. In *Proceedings of the 2020 conference on empirical methods in natural language processing: system demonstrations*, pages 38–45, 2020.
- [58] H. Yan, A. Bombarely, and S. Li. Deepte: a computational method for de novo classification of transposons with convolutional neural network. *Bioinformatics*, 36(15):4269–4275, 2020.
- [59] C. Yang, D. Chowdhury, Z. Zhang, W. K. Cheung, A. Lu, Z. Bian, and L. Zhang. A review of computational tools for generating metagenome-assembled genomes from metagenomic sequencing data. *Computational and Structural Biotechnology Journal*, 19:6301–6314, 2021.
- [60] M. Yang, L. Huang, H. Huang, H. Tang, N. Zhang, H. Yang, J. Wu, and F. Mu. Integrating convolution and self-attention improves language model of human genome for interpreting non-coding regions at base-resolution. *Nucleic acids research*, 50(14):e81–e81, 2022.
- [61] Y. Yang, X. Jiang, B. Chai, L. Ma, B. Li, A. Zhang, J. R. Cole, J. M. Tiedje, and T. Zhang. Args-oap: online analysis pipeline for antibiotic resistance genes detection from metagenomic data using an integrated structured arg-database. *Bioinformatics*, 32(15):2346–2351, 2016.
- [62] Z. Zhang, Z. Han, Y. Wu, S. Jiang, C. Ma, Y. Zhang, and J. Zhang. Metagenomics assembled genome scale analysis revealed the microbial diversity and genetic polymorphism of lactiplantibacillus plantarum in traditional fermented foods of hainan, china. *Food Research International*, 150:110785, 2021.
- [63] Z. Zhou, Y. Ji, W. Li, P. Dutta, R. Davuluri, and H. Liu. Dnabert-2: Efficient foundation model and benchmark for multi-species genome. *arXiv preprint arXiv:2306.15006*, 2023.
- [64] M. Zvyagin, A. Brace, K. Hippe, Y. Deng, B. Zhang, C. O. Bohorquez, A. Clyde, B. Kale, D. Perez-Rivera, H. Ma, et al. Genslms: Genome-scale language models reveal sars-cov-2 evolutionary dynamics. *The International Journal of High Performance Computing Applications*, page 10943420231201154, 2022.

## A Preliminaries

Transformers are the dominant tools for modeling sequence data. In Transformer, the input sequence is first transformed into a series of vectors, each corresponding to an element of the sequence (e.g., a word or character), which are generated by an embedding layer.

Subsequently, self-attention mechanism computes the attention score of each element with respect to the other elements in the sequence. Specifically, by multiplying three different weight matrices, each input vector  $X$  is transformed into: a query vector  $Q$ , a key vector  $K$ , and a value vector  $V$ . Then, the attention score is computed.

$$Attention(Q, K) = \frac{Q \cdot K^T}{\sqrt{d_k}} \quad (6)$$

These scores are normalized by Softmax function, where it is multiplied by the value vector  $V$  to get the weighted value vector. All these weighted value vectors are summed to form the output  $Z$  of the attention layer.

$$Z = softmax(Attention(Q, K))V \quad (7)$$

Transformers typically use a multi-head attention mechanism to capture the information in the sequence more comprehensively. The outputs of each self-attention and feed-forward network layer are passed through a residual connection, followed by layer normalization. After multi-layer processing, the Transformer model outputs a series of vectors suitable for a variety of downstream tasks such as categorization, translation, or text generation of text, speech, or any form of sequence data.

## B Model Configurations

All our experiments are performed on 4 NVIDIA V100 GPUs and the PyTorch framework. The encoder of FGBERT is initialized with Roberta [11]. The parameters for pre-training: batch size = 1000, 19 encoder layers, 10 attention heads, embedding dimension = 1280, and relative position encoding. During the pre-training stage, the model is trained for 500 epochs. We use the AdamW optimizer [35] with a weight decay of 0.02. The learning rate is initialized to 1e-5 and warmed up to 1e-4 after 5000 epochs. Then, it is reduced to 1e-5 by a cosine decay strategy. The overall model comprises 954.73M parameters with a computational load of 2.55B FLOPs.

## C Dataset.

**MGnify dataset** includes genome sequence information from different microbial communities and their Biome Names (e.g., "Engineered", "Host-associated", and "Control"), as well as their corresponding Sample Classes, Sample Numbers, and Spectrum Categories. Lineage Category refers to the taxonomic information of microorganisms, which describes the taxonomic hierarchy of microorganisms from Domain (e.g., "root" or "Engineered") to Species (e.g., "Continuous culture" or "Saliva"), which can be observed in Table 5.

Table 5: Microbial Species and Genomic Data Across Various Environments in the MGnify Dataset. Each column is catalogs, species, and genomes respectively.

| Catalogues         | Species | Genomes |
|--------------------|---------|---------|
| Human gut          | 4744    | 289232  |
| Human oral         | 452     | 1225    |
| Cow rumen          | 2729    | 5578    |
| Marine             | 1496    | 1504    |
| Pig gut            | 1376    | 3972    |
| Zebrafish feacel   | 79      | 101     |
| Non-model fish gut | 172     | 196     |

**E.coil K12 RegulonDB** Information such as the name of the operon, its description, and the name of the genes included in the partially E. coil K12 RegulonDB dataset are listed in Table 6.

**CARD** Table 8 shows a partial list of instances from the CARD dataset, including data IDs, ARO (Antibiotic Resistance Ontology) Accession IDs, AMR (Antimicrobial Resistance) category names, drug category names, and Resistance Mechanism names.

Table 6: Examples of Operons Dataset. Information such as the name of the operon, its description, and the name of the genes included in the partially E. coil K12 RegulonDB dataset

| GeneID | Operon name | Discription Operon name                               | Gene name(s) contained in the operon | Other database's id related to gene |
|--------|-------------|---|--------------------------------------|-------------------------------------|
| 2971   | ygiV        | DNA-binding transcriptional repressor YgiV            | None                                 | None                                |
| 2972   | ygiW        | BOF family protein YgiW                               | None                                 | None                                |
| 2973   | qseB        | DNA-binding transcriptional activator QseB            | qseBC                                | None                                |
| 2974   | qseC        | sensor histidine kinase QseC                          | qseBC                                | None                                |
| 2975   | ygiZ        | DUF2645 domain-containing inner membrane protein YgiZ | None                                 | None                                |
| 2976   | mdaB        | NADPH:quinone oxidoreductase MdaB                     | None                                 | None                                |
| 2977   | ygiN        | putative quinol monooxygenase YgiN                    | None                                 | None                                |
| 2978   | parE        | DNA topoisomerase IV subunit B                        | nudF-yqiB-cpdA-yqiA-parE             | None                                |
| 2979   | yqiA        | esterase YqiA   | nudF-yqiB-cpdA-yqiA-parE             | None                                |
| 2980   | cpdA        | cAMP phosphodiesterase                                | nudF-yqiB-cpdA-yqiA-parE             | None                                |
| 2981   | yqiB        | DUF1249 domain-containing protein YqiB                | nudF-yqiB-cpdA-yqiA-parE             | None                                |
| 2982   | nudF        | ADP-sugar pyrophosphatase                             | nudF-yqiB-cpdA-yqiA-parE             | None                                |
| 2983   | tolC        | outer membrane channel TolC                           | tolC-ygiBC                           | tolC-ygiBC                          |
| 2984   | ygiB        | DUF1190 domain-containing protein YgiB                | tolC-ygiBC                           | tolC-ygiBC                          |
| 2985   | ygiC        | putative acid-amine ligase YgiC                       | tolC-ygiBC                           | tolC-ygiBC                          |
| 2986   | ygiD        | 4,5-DOPA dioxygenase extradiol                        | None                                 | None                                |

Note: This table provides a partial list of instances from the Operons dataset, including Gene data IDs, operon names, descriptions, Gene name(s) contained in the operon, and other database's id related to the gene.

## D Baselines

We evaluate ours compared with three traditional machine learning methods (RandomForest, SVM, KNN), three sequence modeling methods (BiLSTM [52] vs. LSTM [21]), Vanilla Transformer and four pre-trained models on protein/DNA sequences (ESM-2 [33], HyenaDNA [43], NT [10] and DNABERT2 [63]) for comparison. Machine learning methods encode sequences by K-mers, where K takes the best one of the [3,4,5,6] parameters. Sequence modeling methods encode genes using Word2vec. For a fair comparison, each model was trained and optimized to obtain the corresponding optimal hyperparameters. We adopt a 5-fold cross-validation approach to partition all downstream task datasets into a training set (80%), a validation set (10%), and a test set (10%).

## E Evaluation Metrics.

To fully evaluate the model performance, we used several evaluation metrics including Accuracy, Macro Pre, Macro Recall, Macro F1 and Weighted F1.

Precision: indicates the precision rate, which is the ratio of the number of true positive samples to the number of samples classified as positive.  $\text{precision} = \text{TP} / (\text{TP} + \text{FP})$

Recall: the ratio of the number of true positive samples to the number of all positive samples in the sample set,  $\text{Recall} = \text{TP} / (\text{TP} + \text{FN})$

F1score: used to combine Precision and Recall,  $\text{F1-Score} = 2 * \text{Precision} * \text{Recall} / (\text{Precision} + \text{Recall})$

## F Overview of Downstream Tasks

**Operon Prediction Task** is to identify the transcription factor binding sites that have the strongest correlation with operon regulation in the gene regulatory network [9, 13], which helps us to understand the mechanism and network of gene regulation and reveals the key interactions between transcription factors and operons [46]. In general, operons are composed of a set of multiple genes close to each other.

**ARGs and VFs Prediction Task.** Pathogenic microorganisms pose a threat to public health by invading hosts through virulence factors (VFs) and exacerbating antibiotic resistance genes (ARGs) [45]. Despite different evolutionary pathways, VFs and ARGs share common features that are critical for pathogenic bacteria to adapt to and survive in the microbial

environment [38]. Therefore, accurate identification of VFs and ARGs is extremely important for understanding the relationship between the microbiome and disease. However, traditional sequence-matching-based ARG identification methods suffer from high false-positive rates and specific ARG category bias [26, 5]. Existing methods for analyzing metagenomic data are insufficient, especially tools for co-predicting the two are scarce, and also suffer from threshold sensitivity [61]. Therefore, there is an urgent need for deep learning methods to rapidly and accurately predict the presence of VF and ARG in metagenomic datasets.

**Overview of Enzymes.** Enzymes are important catalysts in living cells that produce essential molecules needed by living organisms through chemical reactions [54]. While traditional methods rely on time-consuming and labor-intensive biochemical experiments, advanced technologies such as deep learning can be used to efficiently and accurately predict large-scale genomic data, accelerating biomedical research and new drug development.

**Overview of Pathogens.** Pathogenic bacteria are a group of bacteria that can cause disease and can pose a significant threat to human health compared to commensal non-pathogenic bacteria in the human body with their ability to invade the host and cause disease [27]. The existing methods are limited to long genome sequences and are dominated by short sequence (>3 kb) inputs, which are unable to directly process long genome sequences at the million bp level. Hence, the development of accurate deep learning algorithms for the precise identification of pathogens (causative agents) can help in the development of new therapies and vaccines, and improve the ability to respond to the threat of drug resistance.

**Overview.** The Nitrogen cycle is a collection of important biogeochemical pathways in the Earth’s ecosystems, and quantitatively studying the functional genes related to the N cycle and linking them to environmental and ecological processes is one of the important focuses in environmental genomics research [16]. Currently, macrogenome sequencing has been widely used to characterize gene families involved in N cycling processes. However, existing methods usually face the problems of inefficient database searches, unclear direct lineage classification, and low coverage of N cycle genes and/or gene (sub)families when analyzing N cycle gene families in macrogenomes. Consequently, accurate prediction of the functional categories of genes or proteins related to nitrogen metabolism in microorganisms is important for analyzing important resources in the process of nitrogen cycling and understanding the nitrogen cycle in ecosystems.

## G Detailed Classification Results on CARD Dataset

Table 11: Detailed Classification Results of FGBERT Model on AMR Gene Family Category Prediction. Our model performs a three-class classification prediction task for each gene sequence in the CARD dataset, covering AMR Gene Family (269 classes in total), Drug Class (37 classes in total) and Resistance Mechanism (7 classes in total). In order to comprehensively evaluate the model performance, we used several evaluation metrics, including Accuracy, Macro Pre, Macro Recall, Macro F1, Weighted Pre, Weighted Recall and Weighted F1. One of the challenging tasks is to predict the AMR Gene Family category, which has up to 269 different classes and requires high complexity classification of gene sequences with multiple labels. This requires the model to be able to understand the biological features of the gene sequences and accurately map them to the corresponding AMR Gene Family categories to ensure accurate prediction in the multi-classification task.

| Class Name   | Total Count | Correct Num | Correct Ratio |
|--|-------------|-------------|---------------|
| CTX-M beta-lactamase   | 46          | 46          | 100.00%       |
| ADC beta-lactamases pending classification for carbapenemase activity      | 36          | 36          | 100.00%       |
| CMY beta-lactamase   | 33          | 33          | 100.00%       |
| quinolone resistance protein (qnr)   | 22          | 22          | 100.00%       |
| MCR phosphoethanolamine transferase  | 21          | 20          | 95.24%        |
| major facilitator superfamily (MFS) antibiotic efflux pump                 | 17          | 15          | 88.24%        |
| trimethoprim resistant dihydrofolate reductase dfr                         | 12          | 8           | 66.67%        |
| AAC(6')  | 12          | 12          | 100.00%       |
| CARB beta-lactamase  | 10          | 9           | 90.00%        |
| ADC beta-lactamase without carbapenemase activity                          | 10          | 3           | 30.00%        |
| 16s rRNA with mutation conferring resistance to aminoglycoside antibiotics | 9           | 7           | 77.78%        |
| fosfomycin thiol transferase   | 6           | 3           | 50.00%        |
| ANT(3'')   | 6           | 6           | 100.00%       |
| chloramphenicol acetyltransferase (CAT)                                    | 6           | 5           | 83.33%        |
| 23S rRNA with mutation conferring resistance to macrolide antibiotics      | 5           | 5           | 100.00%       |
| APH(3')  | 4           | 2           | 50.00%        |
| AAC(3)   | 4           | 4           | 100.00%       |
| IND beta-lactamase   | 4           | 4           | 100.00%       |

Continued on next page

**Table 11 – continued from previous page**

| Class Name   | Total Count | Correct Num | Correct Ratio |
|--|-------------|-------------|---------------|
| ATP-binding cassette (ABC) antibiotic efflux pump                                | 4           | 3           | 75.00%        |
| tetracycline-resistant ribosomal protection protein                              | 4           | 3           | 75.00%        |
| IMI beta-lactamase   | 4           | 4           | 100.00%       |
| CfiA beta-lactamase  | 4           | 4           | 100.00%       |
| fluoroquinolone resistant gyrA   | 4           | 2           | 50.00%        |
| 16S rRNA methyltransferase (G1405)   | 3           | 1           | 33.33%        |
| resistance-nodulation-cell division(RND) antibiotic efflux pump                  | 3           | 0           | 0.00%         |
| macrolide phosphotransferase (MPH)   | 3           | 0           | 0.00%         |
| tetracycline inactivation enzyme   | 3           | 3           | 100.00%       |
| fluoroquinolone resistant parC   | 3           | 3           | 100.00%       |
| lincosamide nucleotidyltransferase (LNU)   | 2           | 1           | 50.00%        |
| rifampin ADP-ribosyltransferase (Arr)  | 2           | 2           | 100.00%       |
| CphA beta-lactamase  | 2           | 2           | 100.00%       |
| AAC(2 <sup>+</sup> )   | 2           | 2           | 100.00%       |
| FRI beta-lactamase   | 2           | 2           | 100.00%       |
| HERA beta-lactamase  | 2           | 2           | 100.00%       |
| EC beta-lactamase  | 2           | 2           | 100.00%       |
| nitroimidazole reductase   | 2           | 1           | 50.00%        |
| Target protecting FusB-type protein conferring resistance to Fusidic acid        | 1           | 1           | 100.00%       |
| SME beta-lactamase   | 1           | 1           | 100.00%       |
| Miscellaneous ABC-F subfamily ATP-binding cassette ribosomal protection proteins | 1           | 0           | 0.00%         |
| APH(2 <sup>+</sup> )   | 1           | 0           | 0.00%         |
| CfxA beta-lactamase  | 1           | 1           | 100.00%       |
| SRT beta-lactamase   | 1           | 1           | 100.00%       |
| aminoglycoside bifunctional resistance protein                                   | 1           | 0           | 0.00%         |
| APH(9)   | 1           | 0           | 0.00%         |
| sulfonamide resistant sul  | 1           | 0           | 0.00%         |
| ANT(6)   | 1           | 0           | 0.00%         |
| multidrug and toxic compound extrusion (MATE) transporter                        | 1           | 0           | 0.00%         |
| methicillin resistant PBP2   | 1           | 1           | 100.00%       |
| streptothricin acetyltransferase (SAT)   | 1           | 0           | 0.00%         |
| pmr phosphoethanolamine transferase  | 1           | 1           | 100.00%       |
| BlaZ beta-lactamase  | 1           | 0           | 0.00%         |
| rifampin monooxygenase   | 1           | 0           | 0.00%         |
| APH(6)   | 1           | 0           | 0.00%         |
| macrolide esterase   | 1           | 0           | 0.00%         |
| ANT(4 <sup>+</sup> )   | 1           | 0           | 0.00%         |
| ANT(9)   | 1           | 0           | 0.00%         |
| AQU beta-lactamase   | 1           | 1           | 100.00%       |
| CepA beta-lactamase  | 1           | 1           | 100.00%       |
| APH(3 <sup>+</sup> )   | 1           | 0           | 0.00%         |
| sulfonamide resistant dihydropteroate synthase folP                              | 1           | 0           | 0.00%         |
| aminocoumarin resistant gyrB   | 1           | 0           | 0.00%         |
| fluoroquinolone resistant parE   | 1           | 0           | 0.00%         |
| daptomycin resistant cls   | 1           | 0           | 0.00%         |
| 16s rRNA with mutation conferring resistance to peptide antibiotics              | 1           | 0           | 0.00%         |
| elfamycin resistant EF-Tu  | 1           | 0           | 0.00%         |
| defensin resistant mprF  | 1           | 1           | 100.00%       |
| antibiotic resistant ndh   | 1           | 0           | 0.00%         |
| fluoroquinolone resistant gyrB   | 1           | 0           | 0.00%         |
| 16S rRNA with mutation conferring resistance to tetracycline derivatives         | 1           | 0           | 0.00%         |
| FONA beta-lactamase  | 1           | 1           | 100.00%       |
| antibiotic-resistant isoleucyl-tRNA synthetase (ileS)                            | 1           | 1           | 100.00%       |
| antibiotic-resistant murA transferase  | 1           | 0           | 0.00%         |
| antibiotic-resistant UhpT  | 1           | 1           | 100.00%       |
| small multidrug resistance (SMR)antibiotic efflux pump                           | 1           | 0           | 0.00%         |
| ARL Beta-lactamase   | 1           | 1           | 100.00%       |
| General Bacterial Porin with reduced permeability to peptide antibiotics         | 1           | 0           | 0.00%         |
| CMH beta-lactamase   | 1           | 1           | 100.00%       |
| AXC beta-lactamase   | 1           | 1           | 100.00%       |
| CRH beta-lactamase   | 1           | 1           | 100.00%       |
| KLUC beta-lactamase  | 1           | 1           | 100.00%       |
| LUT beta-lactamase   | 1           | 1           | 100.00%       |
| PFM beta-lactamase   | 1           | 1           | 100.00%       |

Continued on next page

**Table 11 – continued from previous page**

| Class Name         | Total Count | Correct Num | Correct Ratio |
|--------------------|-------------|-------------|---------------|
| SGM beta-lactamase | 1           | 1           | 100.00%       |



Table 8: Examples of CARD Dataset

| Model ID | ARO Accession | AMR Gene Family  | Drug Class                   | Resistance Mechanism          |
|----------|---------------|--|------------------------------|-------------------------------|
| 2        | 3002999       | CblA beta-lactamase  | cephalosporin                | antibiotic inactivation       |
| 5        | 3002867       | trimethoprim resistant dihydrofolate reductase dfr                               | diaminopyrimidine antibiotic | antibiotic target replacement |
| 7        | 3001989       | CTX-M beta-lactamase   | cephalosporin                | antibiotic inactivation       |
| 10       | 3002244       | CARB beta-lactamase  | penam                        | antibiotic inactivation       |
| 20       | 3002012       | CMY beta-lactamase   | cephamycin                   | antibiotic inactivation       |
| 24       | 3003552       | Target protecting FusB-type protein conferring resistance to Fusidic acid        | fusidane antibiotic          | antibiotic target protection  |
| 25       | 3001980       | CTX-M beta-lactamase   | cephalosporin                | antibiotic inactivation       |
| 27       | 3002835       | lincosamide nucleotidyltransferase (LNU)   | lincosamide antibiotic       | antibiotic inactivation       |
| 31       | 3003163       | CTX-M beta-lactamase   | cephalosporin                | antibiotic inactivation       |
| 35       | 3002804       | fosfomycin thiol transferase   | phosphonic acid antibiotic   | antibiotic inactivation       |
| 38       | 3002649       | APH(3')  | aminoglycoside antibiotic    | antibiotic inactivation       |
| 39       | 3002528       | AAC(3)   | aminoglycoside antibiotic    | antibiotic inactivation       |
| 40       | 3002771       | quinolone resistance protein (qnr)   | fluoroquinolone antibiotic   | antibiotic target protection  |
| 41       | 3003198       | 16S rRNA methyltransferase (G1405)   | aminoglycoside antibiotic    | antibiotic target alteration  |
| 46       | 3002125       | CMY beta-lactamase   | cephamycin                   | antibiotic inactivation       |
| 50       | 3002380       | SME beta-lactamase   | carbapenem                   | antibiotic inactivation       |
| 51       | 3002538       | AAC(3)   | aminoglycoside antibiotic    | antibiotic inactivation       |
| 58       | 3002762       | quinolone resistance protein (qnr)   | fluoroquinolone antibiotic   | antibiotic target protection  |
| 60       | 3002795       | quinolone resistance protein (qnr)   | fluoroquinolone antibiotic   | antibiotic target protection  |
| 63       | 3002546       | AAC(6')  | aminoglycoside antibiotic    | antibiotic inactivation       |
| 64       | 3002083       | CMY beta-lactamase   | cephamycin                   | antibiotic inactivation       |
| 69       | 3002620       | ANT(3'')   | aminoglycoside antibiotic    | antibiotic inactivation       |
| 71       | 3002778       | quinolone resistance protein (qnr)   | fluoroquinolone antibiotic   | antibiotic target protection  |
| 75       | 3003026       | fusidic acid inactivation enzyme   | fusidane antibiotic          | antibiotic inactivation       |
| 88       | 3002066       | CMY beta-lactamase   | cephamycin                   | antibiotic inactivation       |
| 92       | 3001904       | CTX-M beta-lactamase   | cephalosporin                | antibiotic inactivation       |
| 94       | 3002092       | CMY beta-lactamase   | cephamycin                   | antibiotic inactivation       |
| 95       | 3002067       | CMY beta-lactamase   | cephamycin                   | antibiotic inactivation       |
| 98       | 3002059       | CMY beta-lactamase   | cephamycin                   | antibiotic inactivation       |
| 99       | 3002753       | quinolone resistance protein (qnr)   | fluoroquinolone antibiotic   | antibiotic target protection  |
| 105      | 3002243       | CARB beta-lactamase  | penam                        | antibiotic inactivation       |
| 106      | 3002681       | chloramphenicol acetyltransferase (CAT)  | phenicol antibiotic          | antibiotic inactivation       |
| 110      | 3002565       | AAC(6')  | aminoglycoside antibiotic    | antibiotic inactivation       |
| 114      | 3003012       | trimethoprim resistant dihydrofolate reductase dfr                               | diaminopyrimidine antibiotic | antibiotic target replacement |
| 116      | 3002733       | quinolone resistance protein (qnr)   | fluoroquinolone antibiotic   | antibiotic target protection  |
| 120      | 3002604       | ANT(3'')   | aminoglycoside antibiotic    | antibiotic inactivation       |
| 124      | 3002263       | IND beta-lactamase   | carbapenem                   | antibiotic inactivation       |
| 128      | 3002828       | Miscellaneous ABC-F subfamily ATP-binding cassette ribosomal protection proteins | macrolide antibiotic         | antibiotic target protection  |
| 129      | 3000198       | fosfomycin thiol transferase   | phosphonic acid antibiotic   | antibiotic inactivation       |
| 130      | 3001972       | CTX-M beta-lactamase   | cephalosporin                | antibiotic inactivation       |

Note: This table provides a partial list of instances from the CARD dataset, including data IDs, ARO (Antibiotic Resistance Ontology) Accession IDs, AMR (Antimicrobial Resistance) category names, drug category names, and Resistance Mechanism names.

Table 10: Detailed Classification Results of FGBERT Model on Drug Class Category Prediction.

| Class Name                      | Total Count | Correctly Num | Correct Ratio |
|---------------------------------|-------------|---------------|---------------|
| cephalosporin                   | 103         | 101           | 98.06%        |
| aminoglycoside antibiotic       | 47          | 37            | 78.72%        |
| cephamycin                      | 34          | 31            | 91.18%        |
| fluoroquinolone antibiotic      | 33          | 27            | 81.82%        |
| carbapenem                      | 31          | 25            | 80.65%        |
| peptide antibiotic              | 30          | 26            | 86.67%        |
| penam                           | 23          | 21            | 91.30%        |
| tetracycline antibiotic         | 16          | 10            | 62.50%        |
| macrolide antibiotic            | 12          | 10            | 83.33%        |
| diaminopyrimidine antibiotic    | 11          | 8             | 72.73%        |
| phenicol antibiotic             | 11          | 6             | 54.55%        |
| phosphonic acid antibiotic      | 10          | 6             | 60.00%        |
| lincosamide antibiotic          | 3           | 0             | 0.00%         |
| rifamycin antibiotic            | 3           | 1             | 33.33%        |
| disinfecting agents antiseptics | 3           | 2             | 66.67%        |
| nitroimidazole antibiotic       | 3           | 1             | 33.33%        |
| aminocoumarin antibiotic        | 2           | 0             | 0.00%         |
| sulfonamide antibiotic          | 2           | 0             | 0.00%         |
| elfamycin antibiotic            | 2           | 2             | 100.00%       |
| isoniazid-like antibiotic       | 2           | 1             | 50.00%        |
| fusidane antibiotic             | 1           | 0             | 0.00%         |
| nucleoside antibiotic           | 1           | 0             | 0.00%         |
| polyamine antibiotic            | 1           | 0             | 0.00%         |
| thioamide antibiotic            | 1           | 0             | 0.00%         |
| glycopeptide antibiotic         | 1           | 0             | 0.00%         |
| mupirocin-like antibiotic       | 1           | 0             | 0.00%         |
| pleuromutilin antibiotic        | 1           | 0             | 0.00%         |
| salicylic acid antibiotic       | 1           | 0             | 0.00%         |